

ALFALFA DISCOVERY OF THE NEARBY GAS-RICH DWARF GALAXY LEO P. III. AN EXTREMELY METAL DEFICIENT GALAXY[†]

EVAN D. SKILLMAN¹, JOHN J. SALZER^{2,3}, DANIELLE A. BERG¹, RICHARD W. POGGE⁴, NATHALIE C. HAURBERG^{2,3}, JOHN M. CANNON^{5,3}, ERIK AVER⁶, KEITH A. OLIVE^{1,7}, RICCARDO GIOVANELLI⁸, MARTHA P. HAYNES⁸, ELIZABETH A.K. ADAMS⁸, KRISTEN B.W. MCQUINN¹, AND KATHERINE L. RHODE²

Accepted for publication in the Astronomical Journal 25 April 2013 (UMN-TH-3126/12, FTPI-MINN-12/37)

ABSTRACT

We present KPNO 4-m and LBT/MODS spectroscopic observations of an H II region in the nearby dwarf irregular galaxy Leo P discovered recently in the Arecibo ALFALFA survey. In both observations, we are able to accurately measure the temperature sensitive [O III] λ 4363 line and determine a “direct” oxygen abundance of $12 + \log(\text{O}/\text{H}) = 7.17 \pm 0.04$. Thus, Leo P is an extremely metal deficient (XMD) galaxy, and, indeed, one of the most metal deficient star-forming galaxies ever observed. For its estimated luminosity, Leo P is consistent with the relationship between luminosity and oxygen abundance seen in nearby dwarf galaxies. Leo P shows normal α element abundance ratios (Ne/O, S/O, and Ar/O) when compared to other XMD galaxies, but elevated N/O, consistent with the “delayed release” hypothesis for N/O abundances. We derive a helium mass fraction of $0.2509^{+0.0184}_{-0.0123}$ which compares well with the WMAP + BBN prediction of 0.2483 ± 0.0002 for the primordial helium abundance. We suggest that surveys of very low mass galaxies compete well with emission line galaxy surveys for finding XMD galaxies. It is possible that XMD galaxies may be divided into two classes: the relatively rare XMD emission line galaxies which are associated with starbursts triggered by infall of low-metallicity gas and the more common, relatively quiescent XMD galaxies like Leo P, with very low chemical abundances due to their intrinsically small masses.

Subject headings: galaxies: abundances - galaxies: dwarf - galaxies: evolution

1. INTRODUCTION

¹ Minnesota Institute for Astrophysics, School of Physics and Astronomy, University of Minnesota, 116 Church St. SE, Minneapolis, MN 55455; skillman@astro.umn.edu, berg@astro.umn.edu, olive@physics.umn.edu, kmcquinn@astro.umn.edu

² Astronomy Department, Indiana University, 727 East 3rd Street, Bloomington, IN 47405; slaz@astro.indiana.edu, nhaurber@astro.indiana.edu, rhode@astro.indiana.edu

³ Visiting Astronomer, Kitt Peak National Observatory, National Optical Astronomy Observatory, which is operated by the Association of Universities for Research in Astronomy (AURA) under cooperative agreement with the National Science Foundation.

⁴ Department of Astronomy, The Ohio State University, 140 W 18th Ave, Columbus, OH 43210, USA; Center for Cosmology and AstroParticle Physics, The Ohio State University, 191 West Woodruff Avenue, Columbus OH 43210; pogge@astronomy.ohio-state.edu

⁵ Department of Physics and Astronomy, Macalester College, Saint Paul, MN 55105; jcannon@macalester.edu

⁶ Department of Physics, Gonzaga University, Spokane, WA 99258; aver@gonzaga.edu

⁷ William I. Fine Theoretical Physics Institute, School of Physics and Astronomy, University of Minnesota, 116 Church St. SE, Minneapolis, MN 55455

⁸ Center for Radiophysics and Space Research, Space Sciences Building, Cornell University, Ithaca, NY 14853; riccardo@astro.cornell.edu, haynes@astro.cornell.edu, betsey@astro.cornell.edu

[†] Some of the observations reported here were obtained at the LBT Observatory. The LBT is an international collaboration among institutions in the United States, Italy, and Germany. LBT Corporation partners are: The University of Arizona on behalf of the Arizona university system; Istituto Nazionale di Astrofisica, Italy; LBT Beteiligungsgesellschaft, Germany, representing the Max-Planck Society, the Astrophysical Institute Potsdam, and Heidelberg University; The Ohio State University, and The Research Corporation, on behalf of The University of Minnesota, The University of Notre Dame, and The University of Virginia.

Metallicity determinations of the interstellar media in galaxies allow us to assess the chemical evolutionary status of a galaxy. In this regard, studies of the lowest metallicity, least chemically evolved galaxies are of special interest (Mateo 1998; Kunth & Östlin 2000; Tolstoy et al. 2009; McConnachie 2012). Specifically, they are important for studies of: (1) star formation at low metallicity, which is critical to understanding star formation in the early universe; (2) stellar properties of low metallicity massive and intermediate mass stars, which provide critical constraints on theories of stellar evolution; (3) constraints on the early enrichment of the pre-galactic medium; and (4) studies of the primordial elemental abundances.

Giovanelli et al. (2013) have reported the discovery of a nearby dwarf irregular galaxy (AGC 208583 = Leo P) as part of the Arecibo Legacy Fast ALFA Survey (ALFALFA, Giovanelli et al. 2005; Haynes et al. 2011). The ALFALFA survey is a blind survey in the HI 21cm line covering 7000 square degrees of high Galactic latitude sky. Leo P was discovered as part of a program to identify mini-halo candidates in the ALFALFA survey (Giovanelli et al. 2010; Adams et al. 2013). Follow-up broadband optical imaging by Rhode et al. (2013) clearly demonstrated the presence of a resolved stellar population at the location of the ALFALFA HI detection, and H α imaging in the same study revealed a strong H α source associated with a bright central star in Leo P.

Here we report on optical spectroscopy of the emission line source in Leo P. We present results of optical spectroscopy from the Kitt Peak National Observatory (KPNO) 4-m and from the Large Binocular Telescope (LBT) in Section 2, and derive H II region physical con-

ditions from the spectra in Section 3. We derive chemical abundances from each of the two spectra in Section 4. We then compare the results of these abundance analyses to similar analyses of low metallicity H II regions in Section 5, and discuss the implications for our understanding of metal poor galaxies in Section 6. Finally, we summarize our conclusions in Section 7.

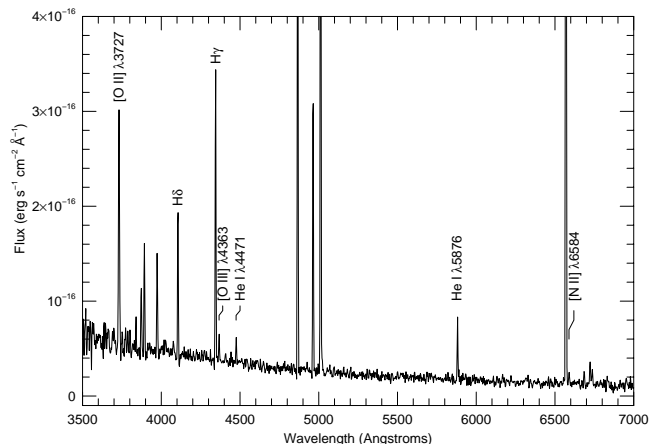


FIG. 1.— The spectrum of the H II region in Leo P taken with the KPNO 4-m. Note the clear detection of the temperature sensitive [O III] λ 4363 emission line and the very weak strength of the [N II] λ 6548,6584 lines, indicative of a very low abundance. H α , H β , and O III λ 5007 are all off scale to allow better visibility of the weaker emission lines.

2. OPTICAL SPECTROSCOPY OF LEO P

2.1. The KPNO 4-m Spectrum

The H II region discovered by Rhode et al. (2013) has coordinates of R.A. = 10:21:45.1 and dec. = +18:05:17.2 (J2000). A spectrum of the Leo P H II region was obtained with the KPNO Mayall 4-m on 2012 April 20 under relatively clear skies and approximately arcsecond seeing. The Ritchey-Chretien Focus Spectrograph was used with a Tektronix 2048² pixel detector (T2KA). A 316 line mm⁻¹ grating (KPC-10A), 1.5'' slit, and WG345 blocking filter were used. This spectroscopic configuration yielded a dispersion of 2.78 Å per pixel, a full width at half maximum resolution of $\lesssim 6$ Å, and a wavelength coverage of 3500–8300 Å. Bias frames, flat-field lamp images, and sky flats were obtained. Combined helium, argon, and neon arc lamps were acquired for accurate wavelength calibration. The spectrophotometric standard star Feige 34 (Massey et al. 1988) was observed before and after the observations of Leo P to yield a secure flux calibration.

Four 1200 second exposures of Leo P were obtained with the slit at a fixed position angle which approximated the parallactic angle at the midpoint of the observations. This, in addition to observing at airmasses of less than ~ 1.2 , served to minimize the wavelength-dependent light loss due to differential refraction (Filippenko 1982).

Standard procedures within the IRAF¹⁰ *ccdred* and

specred packages were used to bias-subtract, flat-field, and illumination-correct the raw data frames. The *lacospec* routine (van Dokkum 2001) was used to remove cosmic rays from the images; this process was checked carefully to ensure that sharp emission lines in our nebular spectra were not accidentally misidentified as cosmic rays by the software. The spectra were then extracted from the 2D images using the IRAF *apextract* package. The individual 1D spectra were wavelength calibrated by applying the solution from the HeArNe comparison lamps, and flux-calibrated using the sensitivity curve derived from the standard star observations. The latter step also involved making airmass-dependent atmospheric extinction and reddening corrections using the standard Kitt Peak extinction curve (Crawford & Barnes 1970). The multiple fully-processed spectra were then combined into a single composite spectrum.

Figure 1 shows the final calibrated 4-m spectrum. Note the clear detection of the temperature sensitive [O III] λ 4363 emission line which allows for a “direct” abundance determination and the very weak strength of the [N II] λ 6548,6584 lines, indicative of a very low metallicity (Denicolò et al. 2002).

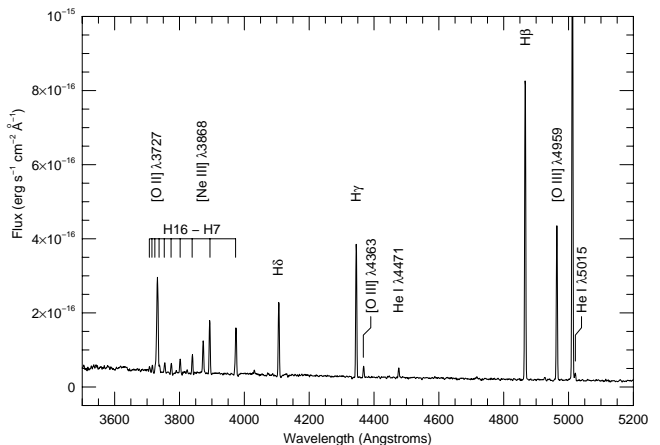


FIG. 2.— The blue portion of the LBT/MODS spectrum of the H II region in Leo P. Note the clear detection of the temperature sensitive [O III] λ 4363 emission line and the detection of the He I λ 5015 line. The higher numbered Balmer series lines are labeled H16 - H7. Note that underlying absorption is not detected for the Balmer lines. O III λ 5007 is off scale to allow better visibility of the weaker emission lines.

2.2. The LBT/MODS Spectrum

After the KPNO 4-m spectrum revealed the very low oxygen abundance of Leo P, we re-observed the H II region in Leo P in order to obtain a higher signal-to-noise spectrum and to detect weak emission lines over a larger wavelength range. A spectrum of the H II region in Leo P was obtained with the Multi-Object Double Spectrograph on the Large Binocular Telescope (LBT/MODS, Pogge et al. 2010) on 2012 April 29 under relatively clear skies and approximately 0.6'' seeing. The LBT/MODS is a double spectrograph with a dichroic that splits the light at ~ 5650 Å and sends it to two separate spectrographs. LBT/MODS1 was used in longslit mode with a 1.0'' slit imaged onto two 3072 \times 8192 format e2v CCDs with 15 μ m (0.12'') pixels. The blue side of MODS1 covers a

¹⁰ IRAF is distributed by the National Optical Astronomy Observatories, which are operated by the Association of Universities for Research in Astronomy, Inc., under cooperative agreement with the National Science Foundation.

wavelength range of 3200 to 5650 Å with a 400 l mm⁻¹ grating providing a resolution of 2.4 Å. The red side of MODS1 covers a wavelength range of 5650 to 10000 Å with a 250 l mm⁻¹ grating providing a resolution of 3.4 Å. Bias frames, flat-field lamp images, and sky flats were obtained. We observed BD+33°2642 and Feige 34 as the standard stars with a 5x60" spectrophotometric slit mask near the parallactic angle. These are from Oke (1990), using the HST CALSPEC flux tables (e.g., Bohlin 2010) which extend further into the UV and Near-IR than the original Oke fluxes. Feige 34 was observed at an airmass that more closely matched the airmass of the target observations, so it was used as a single calibration source instead of being used in combination with BD+33°2642.

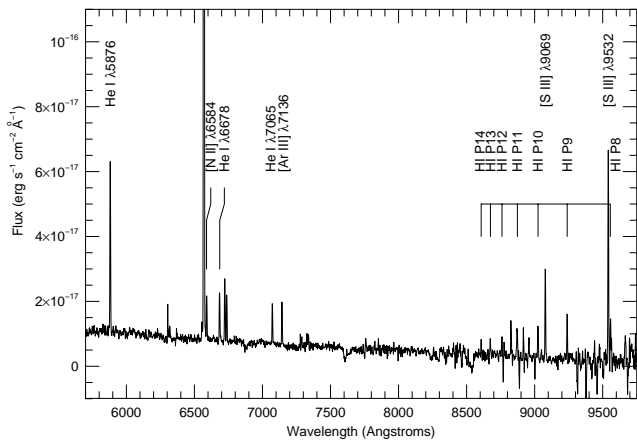


FIG. 3.— The red portion of the LBT/MODS spectrum of the H II region in Leo P. Note the very weak strength of the [N II] $\lambda\lambda 6548, 6584$ lines, indicative of a very low abundance. Also note the detection of the [S III] lines at $\lambda\lambda 9069, 9532$ and the emission lines from the Paschen sequence which are labeled P14 - P8. The noise spikes at wavelengths above $\lambda 8500$ are due to residuals from subtraction of the atmospheric emission lines. $H\alpha$ is off scale to allow better visibility of the weaker emission lines.

Three 900 second exposures were taken at an airmass values less than ~ 1.1 , with the slit at a fixed position angle which approximated the parallactic angle at the midpoint of the observation. Wavelength calibrations were derived from Hg(Ar), Ne, Xe, and Kr lamp spectra taken with the telescope at zenith. MODS is equipped with a closed-loop active flexure compensation system, so only a small ($\lesssim 1\text{Å}$) residual flexure correction, calculated from night-sky lines in the spectra, was applied to the final wavelength calibration.

Standard procedures within the IRAF 2-D package (`twodspec`) were used to bias-subtract, flat-field, and illumination-correct the raw data frames. Airmass dependent atmospheric extinction was corrected using the Kitt Peak (Crawford & Barnes 1970) and Cerro Paranal (Patat et al. 2011) extinction curves corrected approximately to the 3220-meter elevation of Mt. Graham adopting an atmospheric scale height of 7 km.

The multiple sub-exposures were combined, eliminating cosmic rays in the process. The resulting images were then flux-calibrated using the sensitivity curve derived from the standard star observation. Finally, a trace fit to the continuum source in the slit was used to extract the galaxy emission within an aperture that encompassed

$\gtrsim 99\%$ of the light.

In Figure 2 we present the calibrated blue spectrum and in Figure 3 the calibrated red spectrum. Figure 2 shows the clear detection of the Balmer emission line sequence down to H12 at $\lambda 3750$ due to the relatively high sensitivity of LBT/MODS at wavelengths below $\lambda 4000$ (and continuing down to the atmospheric cut-off) and the relatively high spectral resolution. Note also the high significance of the temperature sensitive [O III] $\lambda 4363$ emission line, the detection of the He I $\lambda 5015$ line, and the lack of obvious underlying absorption for the Balmer lines. Figure 3 shows the very weak strength of the [N II] $\lambda\lambda 6548, 6584$ lines, indicative of a very low abundance, detection of He I $\lambda 6678$ at high significance, and the detection of the [S III] lines at $\lambda\lambda 9060, 9532$ with emission lines from the Paschen sequence.

3. EMISSION FLUXES AND PHYSICAL CONDITIONS

3.1. Emission Line Measurements

Emission line strengths were measured from the two spectra using standard methods available within IRAF. In particular, the `splot` routine was used to analyze the extracted one-dimensional spectra and to measure emission line fluxes by integrating under the line. In cases where emission lines were blended, multiple Gaussian profiles were fitted to derive the integrated line fluxes. Special attention was paid to the Balmer lines, which, in some extragalactic H II regions, are located in troughs of significant underlying stellar absorption (e.g., Berg et al. 2011). For Leo P there is very little evidence of underlying absorption. For the bluest Balmer lines, multiple component fits were attempted in which the absorption was fit by a broad, negative Lorentzian profile and the emission was fit by a narrow, positive Gaussian profile. However, even in these cases, the correction for underlying absorption was small, i.e., comparable to the uncertainty in the flux in the line, so simple integration under the line was used.

The errors of the flux measurements were approximated using

$$\sigma_{\lambda} \approx \sqrt{(2 \times \sqrt{N} \times \xi)^2 + (0.02 \times F_{\lambda})^2}, \quad (1)$$

where N is the number of pixels spanning the Gaussian profile fit to the narrow emission lines and ξ is the rms noise in the continuum determined as the average of the rms on each side of an emission line. For weak lines, the uncertainty is dominated by error from the continuum subtraction, so the rms noise term determines the uncertainty. For the lines with flux measurements much stronger than the rms noise of the continuum (usually the $H\alpha$ lines and often the [O III] $\lambda\lambda 4959, 5007$ doublet) the error is dominated by flux calibration and de-reddening uncertainties. In this case, a minimum uncertainty of 2% was assumed (based on the uncertainties in the standard star measurements, Oke 1990), and the right hand term above dominates the uncertainty estimate.

3.2. Reddening Corrections

The relative intensities of the Balmer lines are used to solve for the reddening using the reddening law of Cardelli et al. (1989), assuming $A_V = 3.1 E(B - V)$ and the theoretical case B values from Hummer & Storey

(1987) interpolated to the temperatures derived from the [O III] lines. We used a minimized χ^2 approach to solve simultaneously for the reddening and underlying absorption based on the $H\alpha/H\beta$, $H\gamma/H\beta$, and $H\delta/H\beta$ ratios (cf. Olive & Skillman 2001). The reddenings derived for the two spectra are both very low with $C(H\beta) \lesssim 0.1$. The underlying Balmer absorption is consistent with zero for both spectra. The reddening correction for the LBT/MODS spectrum can be tested by comparing the corrected higher numbered Balmer lines to their theoretical values. The H9 $\lambda 3935$ and H10 $\lambda 3798$ corrected fluxes are consistent with their theoretical ratios to $H\beta$ of 0.074 and 0.054, respectively. The derived values are listed in Table 1. Note that in Section 4.4 we will re-derive the reddening (and other parameters) from the combination of H and He lines.

The foreground reddening in this direction is estimated to be $A_V = 0.07$ magnitudes (Schlafly & Finkbeiner 2011), which is very weak, corresponding to the high Galactic latitude of Leo P ($+54^\circ$). The total reddening in the LBT/MODS spectrum of $C(H\beta) = 0.09$ corresponds to an $A_V \approx 0.2$. This is slightly larger than the expected foreground reddening, indicating only a small amount of reddening internal to the galaxy, in accordance with its very low metallicity (e.g., Cannon et al. 2002, found a value of $A_V = 0.13$ magnitudes of internal extinction in I Zw 18). The relative flux estimates and corresponding errors for the two spectra, corrected for reddening, are listed in Table 1.

Overall, there is good agreement between the relative fluxes in the emission lines. A priori, some small differences are expected due to the difference in slit widths and/or a slight difference in slit placement between the two observations. One small difference occurs for the fainter Balmer lines H11 ($\lambda 3771$), H10 ($\lambda 3798$), H9 ($\lambda 3825$), H8+HeI ($\lambda 3889$), and H7+[Ne III]. For these five emission lines, the KPNO 4-m fluxes are systematically less (though not significantly) than those from the LBT/MODS spectrum. We believe this to be an effect of the very weak underlying H absorption (since observed H absorption is nominally constant in terms of equivalent width, the weakest, i.e., bluest, lines are the most sensitive to the presence of underlying absorption). Because the resolution of the KPNO 4-m spectrum is roughly half that of the LBT/MODS spectrum, the broader underlying absorption will have a greater impact on the H emission line fluxes. The overall consistency between the abundances derived from the two spectra in Section 4 is a direct result of the good agreement between the two spectra.

3.3. Electron Temperature and Density Determinations

For the purpose of deriving nebular abundances, we adopt a simple two zone approximation, where t_2 and t_3 are the electron temperatures (in units of 10^4 K) in the low and high ionization zones respectively. For the high ionization zone, the [O III] $I(\lambda\lambda 4959, 5007)/I(\lambda 4363)$ ratio was used to derive a temperature. We use the 5-level atom calculations available with the IRAF task `temden`. The derived temperatures are given in Table 2. We derive relatively high temperatures of $17,150^{+2040}_{-1390}$ K from the KPNO 4m spectrum and $17,350^{+1390}_{-1060}$ K from the LBT/MODS spectrum, as expected for a low metallicity

H II region. The agreement between the two independent measurements indicates that the H II region in Leo P is clearly very low metallicity.

Because neither the [O II] $\lambda\lambda 7320, 7320$ lines nor the [N II] $\lambda 5755$ line were detected at high significance, we cannot derive a temperature for the low ionization zone directly and, therefore, need to assume a temperature. We used the relation between t_2 and t_3 proposed by Pagel et al. (1992), based on the photoionization modeling of Stasińska (1990) to determine the low ionization zone temperature:

$$t_2^{-1} = 0.5(t_3^{-1} + 0.8). \quad (2)$$

The [S III] $\lambda 6312$ emission line was only detected at the 2σ level, so for the temperature in the [S III] zone we assumed a temperature based on the relationship derived by Garnett (1992):

$$t(S^{+2}) = 0.83(t_3) + 0.17. \quad (3)$$

The low and high ionization region temperatures are tabulated in Table 2.

[S II] $\lambda\lambda 6717, 6731$ and [O II] $\lambda\lambda 3726, 3729$ were used to determine electron densities. These densities are both consistent with the low density limit. The [O II] measurement, which is allowed by the higher resolution of the LBT/MODS spectrograph, provides a stronger constraint on the density due to the lower critical densities of the [O II] emission lines (Osterbrock & Ferland 2006). For all abundance calculations we assume $n_e = 10^2 \text{ cm}^{-3}$ (which is consistent with the 1σ upper bounds and produces identical results for all lower values of n_e).

4. NEBULAR ABUNDANCE ANALYSIS

We analyze both spectra separately, compare the derived abundances, and provide adopted abundances and uncertainties in Table 2. Calculated errors in the abundances provide a statistical estimate only. Additional errors may be important, such as systematic errors due to temperature fluctuations (cf., Peña-Guerrero et al. 2012). However, adopting this approach means that the derived abundances and uncertainties will be directly comparable to most of those reported in the literature.

4.1. Oxygen Abundance Determination

We determine oxygen abundances based on our estimated two zone electron temperatures. Ionic abundances were calculated with:

$$\frac{N(X^i)}{N(H^+)} = \frac{I_{\lambda(i)}}{I_{H\beta}} \frac{j_{H\beta}}{j_{\lambda(i)}}. \quad (4)$$

The emissivity coefficients, which are functions of both temperature and density, were determined using the IONIC routine in IRAF with atomic data updated as reported in Bresolin et al. (2009). This routine applies the 5-level atom approximation, assuming the appropriate ionization zone electron temperature. The total oxygen abundance, O/H, is the sum of O^+/H^+ and O^{++}/H^+ .

The oxygen abundance determinations for Leo P are given in Table 2. We derive an oxygen abundance of $12 + \log(O/H) = 7.17 \pm 0.07$ from the KPNO 4-m spectrum and 7.17 ± 0.05 from the LBT/MODS spectrum. The results from the two spectra are in good agreement, and

we adopt the error weighted average of $12 + \log(\text{O}/\text{H}) = 7.17 \pm 0.04$ as the measurement of the oxygen abundance.

The oxygen abundance in Leo P is one of the lowest oxygen abundances ever derived for an H II region. Formally, the oxygen abundance in Leo P is equivalent to that of the famous low metallicity galaxy I Zw 18 (with $12 + \log(\text{O}/\text{H}) = 7.17 \pm 0.04$; Skillman & Kennicutt 1993; Izotov & Thuan 1999) and lower than that of SBS 0335-052E ($\log(\text{O}/\text{H}) = 7.33 \pm 0.01$; Izotov et al. 1997). It is slightly higher than observed in SBS 0335-052W ($\log(\text{O}/\text{H}) = 7.12 \pm 0.03$; Izotov et al. 2005) and DDO 68 ($\log(\text{O}/\text{H}) = 7.14 \pm 0.03$; Pustilnik et al. 2005; Izotov & Thuan 2007), which are the current record holders.

Note that there are some reports of even lower oxygen abundances in the literature, but these are typically from spectra with lower signal/noise ratios. A small overestimate of the [O III] $\lambda 4363$ line can produce artificially high values of the electron temperature, which translate into lower oxygen abundances. These objects are usually associated with derived electron temperatures well in excess of 20,000 K, which is difficult to achieve in real H II regions, even with only trace amounts of oxygen present.

The significance of the low oxygen abundance in Leo P will be discussed further in Section 6.

4.2. Nitrogen Abundance Determination

We derive the N/O abundance ratio from the [O II] $\lambda 3727$ /[N II] $\lambda 6584$ ratio and assume $\text{N}/\text{O} = \text{N}^+/\text{O}^+$ (Peimbert & Costero 1969). Nava et al. (2006) have investigated the validity of this assumption. They concluded that although it could be improved upon with modern photoionization models, it is valid to within about 10%. Thus, we employ this assumption, mostly for the purposes of direct comparison with other studies in the literature.

The nitrogen to oxygen relative abundance determinations are given in Table 2. For Leo P, $\log(\text{N}/\text{O}) = -1.40 \pm 0.09$ from the KPNO 4-m spectrum and -1.33 ± 0.05 from the LBT/MODS spectrum. Again, there is excellent agreement between the two independent measurements. We adopt an error weighted mean of -1.36 ± 0.04 .

The value of N/O in Leo P is high relative to most determinations of N/O at very low O/H, and significantly higher than the very narrow plateau at -1.60 ± 0.02 which Izotov & Thuan (1999) highlighted in their study of very low metallicity emission line galaxies. This result and its implications for nitrogen nucleosynthesis will be discussed in Section 5.3.

4.3. Neon, Sulfur, and Argon Abundances

To estimate the neon abundance, we assume that $\text{Ne}/\text{O} = \text{Ne}^{++}/\text{O}^{++}$ (Peimbert & Costero 1969). The neon to oxygen relative abundance determinations are given in Table 2. We derive $\log(\text{Ne}/\text{O}) = -0.72 \pm 0.05$ from the KPNO 4-m spectrum and -0.78 ± 0.04 from the LBT/MODS spectrum. These determinations are nearly identical and we adopt -0.76 ± 0.03 as our final determination.

To determine the sulfur and argon abundances, for direct comparison, we adopt the ionization correction fac-

tors (ICF) of Thuan et al. (1995) from H II region photoionization models to correct for the unobserved S^{+3} , Ar^{+2} , and Ar^{+4} states. In the KPNO 4-m spectrum, no [S III] emission lines were detected, so we do not calculate a sulfur abundance as the ICF becomes too uncertain (Garnett 1989), and $\text{Ar}^{+3} \lambda 7136$ was beyond the usable wavelength coverage of the spectrum. Thus, we only have S/O and Ar/O relative abundance measurements from the LBT/MODS spectrum. For $\log(\text{S}/\text{O})$ we obtain -1.49 ± 0.07 and for $\log(\text{Ar}/\text{O})$ we obtain -2.00 ± 0.09 .

4.4. The He Abundance of Leo P from LBT/MODS

The LBT/MODS spectrum of Leo P shows the detection of several He I emission lines at high significance. Thus, we can use the methodology developed in Olive & Skillman (2004) and Aver et al. (2010, 2011) to derive a helium abundance. Specifically, we use a Markov Chain Monte Carlo (MCMC) method to efficiently explore the parameter space in physical conditions (i.e., temperature, density, neutral hydrogen fraction) and other observable effects on the spectrum (i.e., reddening, absorption underlying the H and He emission lines, optical depth in the He emission lines, collisional excitation of H and He emission lines). We use the electron temperature derived from the [O III] emission lines as a prior, in a very conservative manner (see discussion in Aver et al. 2011), producing negligible bias and effectively eliminating non-physical false minima. In this way we determine the helium abundance, the physical parameters, and the uncertainties derived from observations of the nebula.

The LBT/MODS produces spectra with advantages over the spectra typically used to determine nebular He abundances. The vast majority of nebular He abundance determinations in the literature have been derived with a spectral resolution of roughly 6 - 8 Å. The higher resolutions of the LBT/MODS spectrographs (2.4 and 3.4 Å) allow us to directly measure the absorption underlying the H emission lines and, because the resolution is a good match to the intrinsic width of the emission lines, provide optimal sensitivity for the weak emission lines. Additionally, because LBT/MODS is a double spectrograph, all emission lines are observed simultaneously, unlike some spectrographs where one needs to make multiple observations in order to cover the wavelength range at the appropriate spectral resolution. Table 3 presents the fluxes, EWs, and uncertainties for the H and He emission lines used in this analysis.

The methodology developed in Aver et al. (2010, 2011) made use of helium emissivities calculated by Porter et al. (2005, 2007). Thus, in all regards, we follow the methodology of Aver et al. (2010, 2011). For example, H8 and He I $\lambda 3889$ are deblended in a self-consistent way (Aver et al. 2010) accounting for underlying absorption and the equivalent widths of the stellar absorption underlying the He I emission lines are assumed to be equal (Aver et al. 2010). Recently, Porter et al. (2012) have produced a new set of helium emissivities, which, in principle, represent an improvement on the older emissivities. Unfortunately, an error has been discovered in the new emissivities (Porter et al. 2013). We are currently working on a comprehensive paper to determine the effect of these corrected new emissivities on helium abundance calcu-

lations, and an updated analysis of Leo P will appear in that paper. By using the Porter et al. (2005, 2007) emissivities in the present analysis, we can compare the derived He abundance directly to those in the literature in Section 5.4.

Table 4 shows the results of two different helium abundance determinations. The first solution in column 2 is the “standard” analysis, following Aver et al. (2011, 2012), based on 4 H I emission lines (H δ , H γ , H β , and H α) and 6 He I emission lines ($\lambda\lambda$ 3889, 4026, 4471, 5876, 6678, 7065). (Note that in Table 4, this is referred to as nine emission lines because all are referenced to H β .) In column 3, we give the solution after adding in He I λ 5015. The λ 5015 emission line has typically not been used because of its close proximity to [O III] λ 5007 results in a blend at lower resolution. Note, however, that the resolution of the SDSS spectra allowed Izotov et al. (2007) to measure the He I λ 5015 in their very large sample of low metallicity H II regions.

Table 4 shows stable, well-constrained solutions for the physical parameters and the He abundance. As expected, and consistent with previous He abundance analyses, the derived electron temperature of 17,100 K is in excellent agreement with the electron temperature derived from the [O III] emission lines (17,350 K), and significantly higher than the estimated low ionization zone temperature (14,530 K). The electron density is in the low density limit consistent with the [S II] and [O II] emission lines. The reddening, C(H β) is in excellent agreement with that derived from the H lines alone (for this analysis we use the raw fluxes, not corrected for reddening, so the reddening determinations are independent). The solution for the underlying H absorption is in excellent agreement with the number previously derived from the H lines alone. Because the favored value for the optical depth in the He lines is low, the solution is free from assumptions about how the optical depth effects are modeled. Also, the favored solution shows little evidence for neutral H, so the effects of collisional excitation of the lower Balmer lines are also negligible. The χ^2 value of 3.3 (confidence level of 93%) for the “standard” analysis is well within the cut-off of 4.0 per degree of freedom (confidence level of 94.5%) for goodness of fit recommended by Aver et al. (2012).

With the addition of the λ 5015 He I emission line, the solution for the He abundance is essentially unchanged (as might be expected since the line has an observational uncertainty of 20%). However, there is a small decrease in the EW of the underlying He absorption. The addition of λ 5015 is expected to have the greatest impact on the EW of the underlying He absorption because it is an intrinsically weak He I line. Thus, like λ 4026, it is very sensitive to underlying absorption; however, because λ 5015 is a singlet line (unlike λ 4026, which is a triplet line), it is not sensitive to radiative transfer absorption. Note that Izotov et al. (2007) have compared the λ 5015 emission line strength to λ 6678 in their very large sample of low metallicity H II regions, and find generally lower ratios of λ 5015/ λ 6678 when compared to the theoretically expected values. They interpret this as a departure from the standard assumption of case B (resonance lines are optically thick). For this quality of spectrum, (without detection of He I λ 3864) it is not possible to further test the possibility of a departure from

the case B assumption. Our detection of λ 7281, though not strong, is in good agreement with the case B theoretical prediction. Note that if λ 5015 were weaker due to the departure from case B, that we would expect an *increase* in the detected underlying absorption as opposed to the slight decrease which results. Thus, we choose to present an analysis including λ 5015. Adding λ 5015 results in a slightly higher χ^2 of 3.5, and a significantly lower χ^2 per degree of freedom of 1.75 (corresponding to a 83% confidence level).

Two possible concerns for converting a He $^+$ /H $^+$ ratio into a He/H ratio are the presence of He $^{++}$ or the presence of neutral He. The He II λ 4686 emission line is not detected in our spectra at high confidence, indicating that any He $^{++}$ contribution is negligible. Pagel et al. (1992) promoted the use of the “radiation softness parameter”, $\eta \equiv (O^+/S^+)(S^{++}/O^{++})$ (Vilchez & Pagel 1988), as an indication whether a correction for neutral He is warranted. Based on photoionization models with model stellar atmospheres, Pagel et al. (1992) concluded that for values of $\log(\eta) < 0.9$ the correction of neutral He was negligible. From the LBT/MODS spectrum, $\eta = 1.84 \pm 0.64$, which corresponds to $\log(\eta) = 0.26$, well below the region where one needs to make corrections for neutral He. Thus, we will adopt He/H = He $^+$ /H $^+$. The value of He $^+$ /H $^+$ = $0.0837^{+0.0084}_{-0.0054}$ from the last column of Table 4 converts to a value of $0.2509^{+0.0184}_{-0.0123}$ for the He mass fraction.

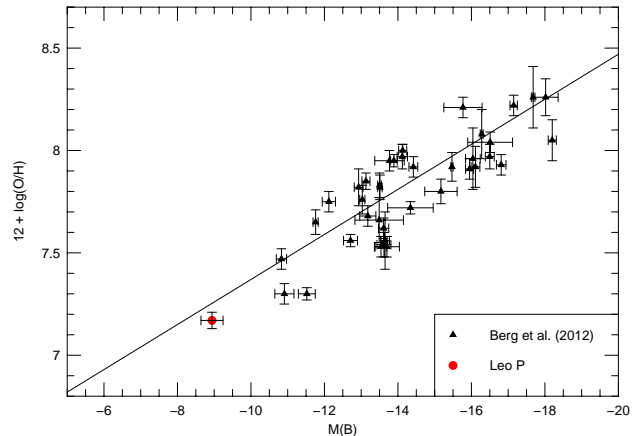


FIG. 4.— The newly derived oxygen abundance and estimated absolute magnitude for Leo P (from Rhode et al. 2013, estimating a distance of 1.75 ± 0.25 Mpc) compared to the B-band luminosity/oxygen abundance relationship for dwarf star forming galaxies from Berg et al. (2012). For the Berg et al. sample, only galaxies with reliable distances (e.g., TRGB distances) and direct abundances were included (i.e., the “Combined Select” sample). The solid line is the regression from Berg et al. (2012).

5. THE SIGNIFICANCE OF THE CHEMICAL ABUNDANCES IN LEO P

5.1. The Luminosity-Metallicity (L - Z) Relationship and Leo P

Although only a single H II region is observed in Leo P, we will assume that the derived abundances are representative of the ISM in the galaxy. This follows from the observation that metallicity gradients and variations are

observed to be small or non-existent in low-mass galaxies (e.g., Skillman et al. 1989a; Kobulnicky & Skillman 1996, 1997; Lee et al. 2006b; Croxall et al. 2009; Berg et al. 2012).

Berg et al. (2012) have compiled a sample of nearby dwarf galaxies with accurate distances measured from either the tip of the red giant branch (TRGB) or Cepheid variable stars and oxygen abundances measured from the “direct” method (their “Combined Select” sample). They have shown that there is relatively low scatter in the relationships between the oxygen abundance with the B-band luminosities, the $4.5 \mu\text{m}$ luminosities, and the masses inferred from infrared luminosity and color. The L-Z relationship is best understood as a fundamental relationship between galaxy mass and chemical abundance (Tremonti et al. 2004). The low abundances in dwarf galaxies reflect inefficient chemical evolution due to large gas mass fractions and the reduced capacity to retain newly synthesized heavy elements.

In Figure 4, using the estimated B-band luminosity of Leo P from Rhode et al. (2013), we compare the position of Leo P with the B-band luminosity/oxygen abundance relationship determined from the “Combined Select” sample by Berg et al. (2012). The uncertainty in the B-band luminosity of Leo P is dominated by the uncertainty in its distance. Rhode et al. (2013) have estimated a distance of roughly between 1.5 and 2.0 Mpc from observations of the resolved stars. This is supported by the distance estimate of $1.3^{+0.9}_{-0.5}$ Mpc derived by Giovanelli et al. (2013) from the baryonic Tully-Fisher relationship. Adopting a distance estimate of 1.75 ± 0.25 Mpc and the photometry from Rhode et al. (2013) results in a B-band luminosity of -8.94 ± 0.30 for Leo P.

Figure 4 shows the excellent agreement between the measurements for Leo P and the L-Z relationship of Berg et al. (2012). In this regard, Leo P represents an extension of this relationship to very low luminosities for actively star forming dwarf galaxies. It would be very valuable to have a more secure distance to Leo P in order to confirm this result. Recent ground-based imaging observations (K. McQuinn, private communication) have been obtained that reach substantially deeper than the WIYN images from Rhode et al. (2013). The RGB is definitively detected in these images, and a preliminary analysis of these new data produce a distance determination that is consistent with the range quoted above. A thorough analysis and presentation of these new observations will be forthcoming. In fact, future observations of distances to other low metallicity objects would be equally valuable¹¹.

The Berg et al. (2012) sample, based on the nearest galaxies, is essentially a volume limited sample. Thus, the relationships from this sample should be representative of typical galaxies (with the exception of galaxies experiencing severe environmental influences). The implication is that the ISM oxygen abundance of a star

¹¹ For example, DDO 68 (also known as UGC 5340), with an estimated distance of ~ 6 Mpc (from brightest stars, Makarova & Karachentsev 1998) and 10 Mpc (after correcting the velocity for the Local Void, Pustilnik & Tepliakova 2011), does not yet have a published TRGB distance. Note that Hubble Space Telescope observations have been acquired (program HST-GO-11578) and a preliminary distance of 12.1 ± 0.7 Mpc has been derived (A. Aloisi, private communication).

forming galaxy is a very strong function of the stellar mass, down to the least massive star forming galaxies known. Given that the luminosity function for galaxies predicts large numbers of these very low mass galaxies, very low metallicity galaxies like Leo P should be quite common. However, the requirement that they possess relatively high surface brightness H II regions for abundance analysis may limit their detectability significantly.

5.2. The α Abundances and Leo P

Figure 5 shows the Ne/O, S/O, and Ar/O relative abundances in Leo P as compared with the relative abundances in emission line galaxies as studied by Izotov & Thuan (1999). For clarity, data points with uncertainties of greater than 0.1 dex have been excluded. Because α element production is thought to be dominated by core collapse supernova production, under the assumption of a universal mass function (IMF), the ratios of the alpha elements are expected to be constant as a function of metallicity. The Ne/O ratio in Leo P is consistent with the mean value and scatter of the very metal poor emission line galaxies shown in Figure 5. The S/O ratio in Leo P is consistent with the scatter seen in the metal poor emission line galaxies. The Ar/O for Leo P appears a bit higher than the typical emission line galaxies, although consistent with the scatter. Given that the ionization correction for Ar/O (Izotov & Thuan 1999) is the most uncertain (the errorbars in the observations do not account for uncertainties in the ionization corrections), at this time we cannot conclude that there is strong evidence for an anomalous Ar/O ratio in Leo P. Note that Stevenson et al. (1993) have suggested that comparing the [Ar III] $\lambda 7136$ emission line to the [S III] $\lambda 9069$ emission line as a measurement of Ar/S may be a more reliable method for testing the stability of relative Ar abundances. Our Ar/S measurement for Leo P of ~ 0.3 is elevated relative to the typical value of 0.2 (Stevenson et al. 1993; Izotov & Thuan 1999), as indicated by Figure 5.

It is well established that both emission line dwarf galaxies and relatively quiescent (or low star formation rate) dwarf galaxies show relatively constant values of Ne/O, S/O, and Ar/O (Thuan et al. 1995; van Zee et al. 1997a; Izotov & Thuan 1999; van Zee & Haynes 2006). This has generally been regarded as expected under the assumption of a universal IMF; however, recent work revealing a trend of lower H α -to-UV flux ratio with decreasing galaxy luminosity has brought that assumption into question for dwarf galaxies (Hoversten & Glazebrook 2008; Meurer et al. 2009; Lee et al. 2009; Boselli et al. 2009). The constancy of the elemental abundance ratios has not played a significant role in this debate, but clearly the observed trends favor a universal IMF. Thus, alternative explanations of the H α -to-UV flux ratio trend assuming a universal IMF (e.g., Fumagalli et al. 2011; Weisz et al. 2012) are likely to be favored, in agreement with the general conclusion of Bastian et al. (2010) that there is little secure evidence supporting a non-universal IMF.

5.3. N/O Relative Abundances and Leo P

Garnett (1990) first showed that the N/O ratio in low metallicity star forming galaxies is relatively constant as

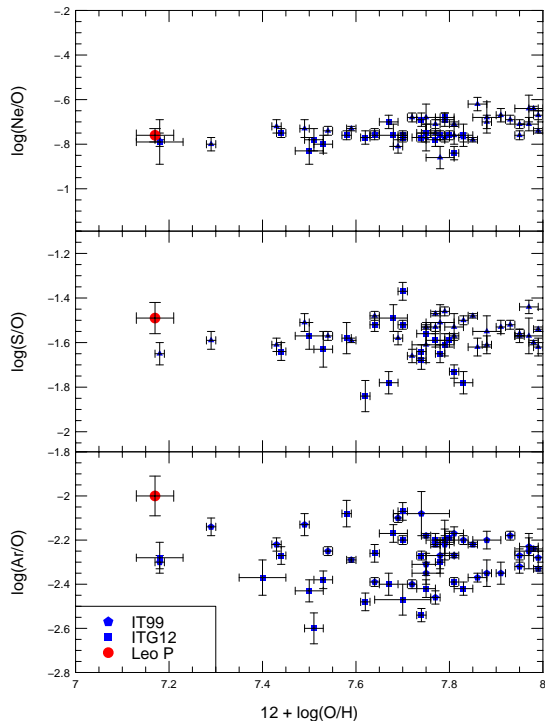


FIG. 5.— The Ne/O, S/O, and Ar/O ratios in Leo P compared to the observed ratios in emission line galaxies from the samples of Izotov & Thuan (1999) and Izotov et al. (2012). Data points with uncertainties of greater than 0.1 dex have been excluded for clarity. Note that all three panels have a y-axis range of 1 dex.

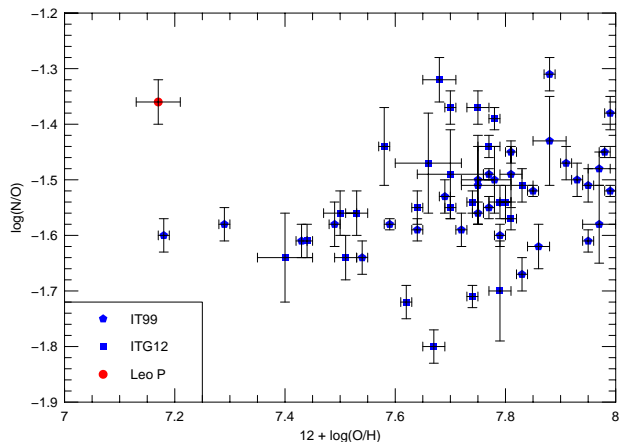


FIG. 6.— The N/O ratio in Leo P compared to the observed ratios in emission line galaxies from the samples of Izotov & Thuan (1999) and Izotov et al. (2012). Note that Leo P lies significantly above the very narrow plateau at $\log(\text{N}/\text{O}) \approx -1.6$ for the emission line galaxies with $12 + \log(\text{O}/\text{H}) < 7.6$ previously noted by Izotov & Thuan (1999). This indicates the likely presence of a secondary component of N in Leo P.

a function of O/H (with a mean value of $\log(\text{N}/\text{O}) = -1.46^{+0.10}_{-0.13}$ for these “plateau” objects). Although the mean is well defined, Garnett (1990) also pointed out that the scatter in N/O at a given O/H is larger than can be accounted for in terms of observational errors. He suggested that the relatively large scatter in N/O at low O/H could be understood in terms of the different delivery times of N and O. That is, O production is under-

stood to be dominated by primary nucleosynthesis from massive stars and delivered early after a star formation event; N can be produced by massive stars (and delivered early with the primary oxygen) and by intermediate mass stars (and delivered relatively later). N can have both primary and secondary origins. Thus, in a galaxy where the N/O ratio has been elevated from its initial N/O ratio from massive stars by contributions from delayed nitrogen from intermediate mass stars, a burst of star formation will drive a galaxy to higher values of O and lower values of N/O, but later contributions from intermediate mass stars will raise the N/O at a constant O/H. At higher metallicities (i.e., $12 + \log(\text{O}/\text{H}) \geq 8.0$), the average N/O rises with increasing O/H, and this is thought to be indicative of the increasing influence of secondary nitrogen production (Pagel 1985). This hypothesis has been supported quantitatively by simple models of galaxy chemical evolution by, e.g., Matteucci & Tosi (1985), Pilyugin (1993), and Fields & Olive (1998).

In a subsequent study of blue compact dwarf galaxies, Izotov & Thuan (1999) drew attention to a different plateau with a very small dispersion (0.02 dex) in $\log(\text{N}/\text{O})$ (with a central value of -1.60) in the extremely metal-poor galaxies with $12 + \log(\text{O}/\text{H}) \leq 7.6$. They proposed that the absence of time-delayed secondary production of N (and C) is consistent with the scenario that extremely metal-poor galaxies are now undergoing their first burst of star formation, and that they are therefore young, with ages not exceeding 40 Myr. They further asserted that this countered the commonly held belief that C and N are produced by intermediate-mass stars at very low metallicities (as these stars would not have yet completed their evolution in these lowest metallicity galaxies).

Later, van Zee & Haynes (2006) derived an average of $\log(\text{N}/\text{O}) = -1.41$ for a sample of isolated dwarf irregular galaxies. Their sample included extremely metal-poor objects, but there was no evidence for the very narrow plateau in N/O at $12 + \log(\text{O}/\text{H}) \leq 7.6$ observed in blue compact galaxies by Izotov & Thuan (1999). Interestingly, all of the extremely metal poor H II regions had N/O values in agreement with the average value of $\log(\text{N}/\text{O}) = -1.41$. Nava et al. (2006) revisited the observed N/O plateau with a large set of objects and determined a mean value for the N/O plateau of $\log(\text{N}/\text{O}) = -1.43$ with a standard deviation of $^{+0.071}_{-0.084}$. They further concluded from a χ^2 analysis that only a small fraction of the observed scatter in N/O is intrinsic. Based on a Monte Carlo analysis of the scatter in the N/O versus O/H diagram, Henry et al. (2006) concluded that one could not distinguish between a delayed nitrogen hypothesis or the hypothesis that nitrogen is produced by massive stars alone at low metallicity. They did conclude that allowing galaxy ages below 250 Myr could not explain the plateau morphology.

Figure 6 shows the N/O relative abundance in Leo P as compared with the N/O relative abundances in emission line galaxies as studied by Izotov & Thuan (1999) and a new sample available from Izotov et al. (2012). For clarity, the emission line galaxy samples have been trimmed of objects with uncertainties in $\log(\text{N}/\text{O})$ of more than 0.1 dex. Clearly, Leo P lies well above the very narrow plateau identified in extremely metal poor emission line

galaxies by Izotov & Thuan (1999).

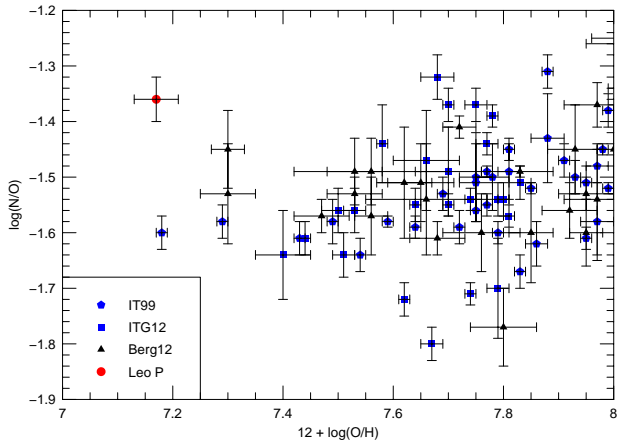


FIG. 7.— The N/O ratio in Leo P compared to the observed ratios in emission line galaxies from the samples of Izotov & Thuan (1999) and Izotov et al. (2012) and the nearby dwarf galaxies from the sample of Berg et al. (2012). Note the larger spread in $\log(\text{N/O})$ at low values of $\log(\text{O/H})$ for the nearby galaxies sample and that the scatter in $\log(\text{N/O})$ at higher values of $\log(\text{O/H})$ for the nearby galaxies is comparable to that of the emission line galaxies.

On the other hand, the N/O abundance for Leo P lies within the scatter observed by Garnett (1990) and van Zee & Haynes (2006). In Figure 7, we have added the galaxies from the sample of Berg et al. (2012) (again limited to those with uncertainties in $\log(\text{N/O})$ less than 0.1 dex). In this diagram, the evidence for a very narrow plateau at values of $12 + \log(\text{O/H}) \leq 7.6$ is not seen. Thus, the very narrow plateau seen in the emission line galaxies cannot be simply a function of metallicity. van Zee et al. (2006) and Berg et al. (2012) point out that there are nearby galaxies with values of $12 + \log(\text{O/H}) \leq 7.6$ and detailed star formation histories (derived from *Hubble Space Telescope* observations of their resolved stars) that clearly show that the bulk of their star formation occurred well before the last 40 Myr (i.e., Leo A and GR 8, Tolstoy et al. 1998; Cole et al. 2007; Dohm-Palmer et al. 1998; Weisz et al. 2011). This implies that the young galaxy hypothesis is not a valid explanation for the plateau in N/O at low metallicity.

With the addition of Leo P, it now looks as though even the most metal poor galaxies show a range in N/O. If the scatter in the $\log(\text{N/O})$ vs $12 + \log(\text{O/H})$ diagram is due to the time delay between producing oxygen and secondary nitrogen as proposed by Garnett (1990), then it could be that the N/O in Leo P is offset to a higher value due to a long period of relative quiescence in which the nitrogen production is allowed to essentially complete before the next round of oxygen production. That two of the three very low metallicity nearby galaxies in Figure 7 lie above the very narrow plateau is interesting. Note that under the interpretation that the scatter is due to secondary nitrogen production, then the *lowest* values of N/O (not the mean value) represent the ratio of N/O in primary nucleosynthesis by massive stars.

van Zee & Haynes (2006) looked at several variables for their possible influence on N/O abundance. In particular, they found a correlation between N/O and color, in the sense that redder galaxies have higher N/O. This sup-

ports the delayed release hypothesis of Garnett (1990), as currently quiescent galaxies would be expected to have, on average, higher values of N/O. Berg et al. (2012) recovered this trend in their sample. For the B-V color of 0.36 for Leo P (Rhode et al. 2013), the relationship between B-V color and N/O determined by Berg et al. (2012) predicts a value of $\log(\text{N/O}) = -1.50$. Although, formally, this is not consistent with our value of -1.36 ± 0.04 , Leo P falls well within the scatter in the relationship, which has an intrinsic dispersion of 0.14 dex, and thus, follows the trend.

The question raised by the N/O versus O/H diagnostic diagram is whether emission line galaxies and relatively quiescent dwarf galaxies occupy different sections of this diagram and therefore represent different chemical evolution paths. Within the literature there are proponents of the view that emission line galaxies (or blue compact galaxies) are intrinsically different from relatively quiescent galaxies, and there are others who allow for the interpretation that emission line galaxies represent a phase that many, or perhaps all, dwarf galaxies can pass through. In the former interpretation, the comparison of relatively quiescent dwarfs with emission line galaxies could be viewed as comparing two different families of galaxies. The emission line galaxies could represent a more homogeneous sample due to the fully populated IMFs normally associated with massive star formation events. For the latter interpretation, all of the points in the diagnostic diagram are directly comparable, although the lower SFRs of relatively quiescent dwarfs are often associated with under-abundances of massive stars due to stochastic effects. Unfortunately there are few high-quality spectra available for extremely low-metallicity galaxies. Adding new observations remains a worthwhile enterprise. The cause of the very narrow plateau in N/O in very low metallicity emission line galaxies is still lacking a definitive explanation, and we will return to this in Section 6.2.

5.4. Leo P and the Primordial Helium Abundance

Next to the cosmic microwave background radiation, standard big bang nucleosynthesis (SBBN) is the most robust probe of the early universe available (e.g., Walker et al. 1991). Furthermore, using the precise baryon density as determined by WMAP (Komatsu et al. 2011), SBBN has effectively become a parameter-free theory (Cyburt et al. 2002). As such, one can use SBBN to make relatively precise predictions of the initial light element abundances of D, ^3He , ^4He , and ^7Li . Therefore, an observational determination of these abundances becomes a test of the concordance between SBBN theory and the analyses of microwave background anisotropies. To test these predictions, the observed abundances must be determined with high precision. Unfortunately, there is a logarithmic relationship between the baryon to photon ratio, η , and the primordial helium abundance, Y_p . Thus, any meaningful test of the theory requires a determination of Y_p to an accuracy of a few percent. The 7-year WMAP value for η is $(6.16 \pm 0.15) \times 10^{-10}$ (Komatsu et al. 2011). Using the procedures of Cyburt et al. (2008), and assuming a neutron mean life of 885.7 ± 0.8 s (Nakamura et al. 2010), this translates to $Y_p = 0.2483 \pm 0.0002$,

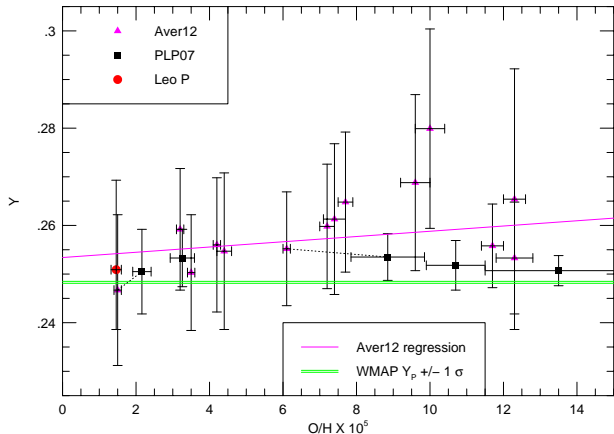


FIG. 8.— The helium mass fraction (Y) and oxygen abundance for Leo P compared to the abundances in emission line galaxies from the sample of Izotov et al. (2007) as analyzed by Aver et al. (2012, Aver12) and the sample from Peimbert et al. (2007, PLP07). The single line is the regression to the data from Aver et al. (2012). Note that the low value of O/H and the comparable error in Y for Leo P make this an important contribution in the determination of the primordial He abundance. Two of the galaxies are common to both comparison samples, I Zw 18 (at low O/H) and Haro 29 (also known as I Zw 36 and Mrk 209, at intermediate O/H) and their points are connected by dotted lines. The narrow band marked WMAP7 is the range of values ($\pm 1\sigma$) estimated for the primordial helium abundance following the calculation by Cyburt et al. (2008) from the 7-year WMAP value for the baryon-to-photon ratio (Komatsu et al. 2011) and assuming the neutron mean life from the Particle Data Group collaboration (Nakamura et al. 2010).

a relative uncertainty of only 0.08%¹².

To date, the favored independent method of determining Y_p uses observations of low metallicity H II regions in dwarf galaxies. By fitting the helium abundance versus metallicity, one can extrapolate back to very low metallicity, corresponding to the primordial helium abundance (Peimbert & Torres-Peimbert 1974). The oxygen to hydrogen ratio, O/H , commonly serves as a proxy for metallicity. The difficulties in calculating an accurate and precise measure of the primordial helium abundance are well established (Olive & Skillman 2001, 2004; Aver et al. 2011; Izotov et al. 2007; Peimbert et al. 2007).

Figure 8 shows the helium mass fraction (Y) and oxygen abundance for Leo P compared to the abundances in emission line galaxies from the sample of Izotov et al. (2007) as analyzed by Aver et al. (2012) and the sample of very high quality spectra analyzed by Peimbert et al. (2007). The two comparison data sets should be directly comparable in that they use identical atomic data for converting relative emission line fluxes into abundances (e.g., Porter et al. 2005, 2007). However, the methodologies for determining physical conditions vary somewhat. For example, two of the galaxies are common to both comparison samples, I Zw 18 and Haro 29 (also known as I Zw 36 or Mrk 209). These two galaxies are connected by solid lines in Figure 8, and one can see that the values for O/H are significantly different (due primarily to assumptions about the effects of temperature variations within the nebulae). We are not advocating that the dif-

¹² Note that the Planck Collaboration has just published a new prediction of the primordial Helium abundance of 0.24771 ± 0.00014 , corresponding to an uncertainty of 0.06% (Ade et al. 2013).

ferent samples be combined, but are only conducting the comparison to show the potential impact of Leo P on determinations of Y_p .

Note that the low value of O/H and uncertainties in He/H which are comparable to the other best studied nebulae in the literature make Leo P an important contribution in the determination of Y_p . To demonstrate this, we calculated a regression of Y on O/H by adding our Leo P He abundance determination to the sample from Aver et al. (2012). This reduced the intercept (Y_p) by roughly 0.3% from 0.2534 to 0.2527 and the error on the intercept by roughly 8% from 0.0083 to 0.0076. The resulting regression of

$$Y = 0.2527 \pm 0.0076 + 61 \pm 92(O/H) \quad (5)$$

has a χ^2 of 2.9.

The value of Y_p implied by the 7-year WMAP observations is indicated in Figure 8. Note, especially, that our determination of Y for Leo P is in excellent agreement with the two determinations for Y in I Zw 18 and that all three are in excellent agreement with the 7-year WMAP prediction for Y_p . Recently, Izotov & Thuan (2010) reported a significant difference between the value of Y_p derived from observations of metal poor H II regions and the value calculated from the cosmic microwave background observations and suggested this was evidence for non-standard Big Bang Nucleosynthesis. From the present analysis of the most metal poor H II regions, we see no motivation for non-standard Big Bang Nucleosynthesis.

6. LEO P AND XMD GALAXIES

6.1. The Search for Extremely Low Metallicity Galaxies

In an overview of the most metal-poor galaxies, Kunth & Östlin (2000) defined “very metal deficient” galaxies as those with metallicities of ten percent of the solar value or less. At the time, the solar value for the oxygen abundance was generally accepted to be $12 + \log(O/H) = 8.91$. In the last decade, there has been a consensus that the solar oxygen abundance is lower than previously thought (e.g., $12 + \log(O/H) = 8.69 \pm 0.05$, Asplund et al. 2009) and recent papers have adopted the definition of an “extremely metal deficient” (XMD) galaxy as having $12 + \log(O/H) \leq 7.65$ (e.g., Kniazev et al. 2003; Pustilnik & Martin 2007; Kakazu et al. 2007; Ekta et al. 2008; Brown et al. 2008; Ekta & Chengalur 2010b).

Also, in the last decade, there have been several programs with the aim of discovering more XMD galaxies. The majority of these programs have concentrated on surveying emission line galaxies. Examples include Kniazev et al. (2000); Ugryumov et al. (2003); Kniazev et al. (2003); Melbourne et al. (2004); Izotov et al. (2006); Papaderos et al. (2008); Brown et al. (2008); Guseva et al. (2011). I Zw 18 (Searle & Sargent 1972) and SBS 0335-052 (Izotov et al. 1990) represent prototypes for XMD galaxies that can be found in emission line surveys. Recently, direct oxygen abundance measurements have been extended to higher redshifts (Hu et al. 2009; Xia et al. 2012). It is interesting that while recent surveys have significantly enlarged the number of metal-poor galaxies, only a few XMD galaxies with oxygen abundances below $\sim 5\%$ of the solar value are known, and no galaxies with abundance below $12 + \log(O/H) \approx 7$ have been

discovered in the Local Volume.

Despite the many surveys of emission line galaxies, the number of XMD galaxies remains small. Searching via emission line surveys provides an extremely low yield. As reported in Izotov et al. (2012), of one million SDSS spectra, 13,000 emission line objects have detectable [O III] $\lambda 4363$, and, of these, there are only 15 candidates with $12 + \log(\text{O}/\text{H}) \leq 7.35$.

An alternate approach to finding low metallicity galaxies relies on the fundamental L-Z relationship between galaxian stellar luminosity (or mass) and abundance for low redshift dwarf galaxies as discussed in Section 5.1 (e.g., Peimbert & Spinrad 1970; Lequeux et al. 1979; Skillman et al. 1989a; Lee et al. 2006a; Berg et al. 2012). Because of the galaxy luminosity function, XMD galaxies are very numerous. However, in part because of their small sizes, XMD galaxies with luminous, high surface brightness star forming regions are rare. The result is an extreme paucity of XMD galaxies in emission line surveys. Many XMD galaxies have been found in surveys of nearby, low luminosity galaxies. XMD galaxies such as Leo A (Skillman et al. 1989a; van Zee et al. 2006), SagDIG (Skillman et al. 1989b; Saviane et al. 2002), UGCA 292 (van Zee 2000), DDO 68 (Pustilnik et al. 2005), and two XMD galaxies in the Lynx-Cancer void (Pustilnik et al. 2011) have been found in this way. Spectroscopic follow-up of $\text{H}\alpha$ surveys of low luminosity galaxies and galaxies discovered in blind H I surveys continue to be very promising in this regard (e.g., Cannon et al. 2011). Surveys like ALFALFA have discovered hundreds of objects whose properties may be confirmed by subsequent follow-up observations to be consistent with those of nearby, low-luminosity dwarf galaxies. A dedicated program to measure the nebular abundances of these galaxies may be very fruitful in discovering new XMD galaxies.

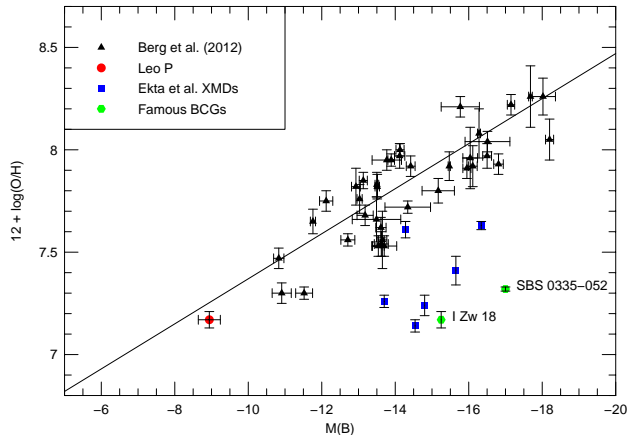


FIG. 9.— Figure 4 is reproduced showing the positions of the famous XMD blue compact galaxies I Zw 18 and SBS 0335-052 relative to the B-band luminosity/oxygen abundance relationship for dwarf star forming galaxies from Berg et al. (2012). The XMD galaxies with disturbed kinematics as observed by Ekta et al. (2006, 2008); Ekta & Chengalur (2010a) are also shown. Note the large offsets of the XMD emission line galaxies from the luminosity/oxygen abundance relationship defined by dwarf star forming galaxies.

6.2. XMD Galaxies and the Infall of Metal-Poor Gas

It is well-established that many of the XMD emission line galaxies lie well off the L-Z relationship for dwarf galaxies. This includes the two best-known XMD galaxies, I Zw 18 and SBS 0335-052. In Figure 9 we have reproduced the L-Z diagram shown in Figure 4, and added I Zw 18 and SBS 0335-052. For I Zw 18, we have used the new distance of Aloisi et al. (2007) and the abundances for the NW component from Skillman & Kennicutt (1993) which is identical to that reported by Izotov et al. (1999). For SBS 0335-052, we have plotted the eastern (luminous) component assuming a distance of 54 Mpc and used the oxygen abundance from Izotov et al. (1999). In Figure 9 it is clear that these two galaxies lie off the L-Z relationship by about 7 magnitudes (or 0.7 dex in $\log(\text{O}/\text{H})$). These offsets are much too large to be attributable to increases in the luminosity due to the present starburst.

Based on new H I observations of XMD galaxies, Ekta & Chengalur (2010b) have proposed that inflow of metal-poor gas from the outskirts of a galaxy to the central star-forming regions (in the case of interaction), or cold gas accretion is the probable cause for the observed low emission-line metallicities of XMD galaxies. This hypothesis is very appealing because it solves two problems simultaneously. It explains how small systems can achieve such high star formation rates that they become visible as emission line galaxies. It also explains why so many of these galaxies do not follow the metallicity/luminosity relationship observed for normal dwarf galaxies in volume limited surveys.

Note that it is also possible to have very low abundances in galaxies through metal-enriched outflows. This is not as appealing as the Ekta & Chengalur (2010b) hypothesis because this would require that the majority of nucleosynthesis in the XMD emission line galaxies is associated with strong bursts of star formation resulting in galactic winds. Furthermore, this does not explain why other galaxies at similar masses have been able to enrich to higher metallicities.

In Figure 9, we have also added in the XMD galaxies with disturbed kinematics as observed by Ekta et al. (2006, 2008) and Ekta & Chengalur (2010a). Here one can see similarly large offsets of the XMD galaxies from the luminosity/oxygen abundance relationship defined by dwarf star forming galaxies. Although offsets from the L-Z relationship for XMD emission line galaxies are well known, what Ekta and collaborators have added is the observation that all of these galaxies have disturbed kinematics indicative of either interaction or infall. In support of this hypothesis, I Zw 18 and SBS 0335-052 are both known to be associated with disturbed H I kinematics (van Zee et al. 1998; Lelli et al. 2012; Pustilnik et al. 1997; Ekta et al. 2009).

It would be very satisfying if this hypothesis could also explain the very narrow plateau seen in the N/O abundances in XMD emission line galaxies. One could hypothesize that if the XMD galaxies are being polluted by relatively pristine gas, and if that pristine gas had a single value of N/O, then XMD emission line galaxies would tend to have similar values of N/O. Unfortunately, absorption line studies of damped Lyman- α systems do not show a universal value of N/O; in fact they show a

very large range in N/O at low values of O/H (Pettini et al. 2008) (which, interestingly, has been used as evidence for a non-universal IMF, Tsujimoto & Bekki 2011). If all emission line XMD galaxies are the products of strong interactions and infall, then it makes the very narrow plateau seen in the N/O abundances in XMD emission line galaxies even more difficult to understand.

The discovery of Leo P supports the hypothesis that XMD line galaxies represent starbursts which are likely triggered by interaction with a companion or infall from an H I cloud, while relatively “quiescent” (i.e., galaxies with low, but non-zero star formation rates) dwarf XMD galaxies are formed through normal evolution of very low mass galaxies.

7. CONCLUSIONS

We have presented KPNO 4-m and LBT/MODS spectroscopic observations of an H II region in the nearby dwarf irregular galaxy Leo P which was discovered recently in the Arecibo ALFALFA survey. The results from both observations are in excellent agreement. The KPNO and LBT observations yield accurate measurements of the temperature sensitive [O III] λ 4363 line and a “direct” oxygen abundance of $12 + \log(\text{O}/\text{H}) = 7.17 \pm 0.04$. This oxygen abundance is among the lowest ever measured in an H II region. Thus, Leo P is an extremely metal deficient (XMD) galaxy.

For its estimated luminosity, Leo P is consistent with the relationship between luminosity and oxygen abundance seen in nearby dwarf galaxies. Future observations of distances of nearby XMD galaxies will help to confirm that the relationship between luminosity and oxygen abundance extends down to the least massive star forming galaxies known.

Leo P shows normal α element abundances (Ne/O, S/O, and Ar/O) when compared to other XMD galaxies. These well-defined trends in the lowest metallicity galaxies are supportive of the hypothesis of a universal initial mass function.

The N/O ratio in Leo P is elevated relative to similarly low metallicity emission line galaxies, but within the scatter seen in observations of large samples of dwarf galaxies. The elevated N/O and optical color of Leo P are consistent with the “delayed release” hypothesis for N/O abundances.

The high signal/noise ratio and spectral resolution of the LBT/MODS spectrum allow us to derive a helium abundance with a precision of $\sim 5\%$. We derive a helium mass fraction of $0.2509^{+0.0184}_{-0.0123}$ which compares well with the WMAP + BBN prediction of 0.2483 ± 0.0002 for the primordial helium abundance. Supplementing the Leo P observations with similar quality spectra of other XMD galaxies will allow a future determination of the primordial helium abundance with an accuracy of less than two percent.

The discovery of Leo P suggests that surveys of very low mass galaxies compete well with emission line galaxy surveys for finding XMD galaxies. With present and future blind H I surveys producing large numbers of low mass galaxies, it should be possible to greatly increase the number of studies of abundances in XMD galaxies.

It is possible that XMD galaxies may be divided into

two classes. The XMD emission line galaxies are rare. This may be attributable to the uncommon occurrence of starbursts triggered by infall or interaction. Because of the galaxy luminosity function (which indicates large numbers of very low mass galaxies) and the relationship between galaxy stellar mass and oxygen abundance, XMD galaxies with very low chemical abundances due to their intrinsically small masses should be common.

Our ability to observe the XMD galaxies with intrinsically small masses may be limited by their low star formation rates and the relatively short lives of the massive stars that produce the observable H II regions. Alternately, their intrinsically low luminosities may prevent them from inclusion in most galaxy catalogs. For example, the H α imaging survey of galaxies in the local 11 Mpc volume by Kennicutt et al. (2008) had an apparent magnitude cut-off of $m_B \leq 15$. With an m_B of 17.3 (Rhode et al. 2013), Leo P is more than 2 magnitudes fainter than this cut-off. Blind H I studies may be the only efficient way to detect these low luminosity XMD galaxies.

We are grateful to Fabio Bresolin for providing his updated atomic data used in deriving the abundances. We are also grateful for helpful input from Antonio Peimbert, Dick Henry, and Simon Pustilnik. We wish to thank the referee for a very helpful and prompt review which led to significant improvements in our paper. EDS is grateful for partial support from the University of Minnesota and NSF Grant AST-1109066. DAB is grateful for support from a Penrose Fellowship, a NASA Space Grant Fellowship, and a Dissertation Fellowship from the University of Minnesota. RWP is supported in part by NSF Grant AST-1108693. JMC is supported by NSF Grant AST-1211683. KAO is supported in part by DOE grant DE-FG02-94ER-40823. The ALFALFA team at Cornell is supported by NSF grants AST-0607007 and AST-1107390 to RG and MPH and by grants from the Brinson Foundation. EAKA is supported by an NSF predoctoral fellowship. KLR is supported by an NSF Faculty Early Career Development (CAREER) award (AST-0847109).

Observations reported here were obtained at the LBT Observatory, a joint facility of the Smithsonian Institution and the University of Arizona. LBT observations were obtained as part of the University of Minnesota’s guaranteed time on Steward Observatory facilities through membership in the Research Corporation and its support for the Large Binocular Telescope, and granted by NOAO, through the Telescope System Instrumentation Program (TSIP). TSIP is funded by the National Science Foundation. This paper uses data taken with the MODS spectrographs built with funding from NSF grant AST-9987045 and the NSF Telescope System Instrumentation Program (TSIP), with additional funds from the Ohio Board of Regents and the Ohio State University Office of Research.

This research has made use of NASA’s Astrophysics Data System Bibliographic Services and the NASA/IPAC Extragalactic Database (NED), which is operated by the Jet Propulsion Laboratory, California Institute of Technology, under contract with the National Aeronautics and Space Administration.

REFERENCES

- Adams, E. A. K., Giovanelli, R., & Haynes, M. P. 2013, *ApJ*, in press, arXiv:1303.6967
- Ade, P. A. R., et al. 2013, arXiv:1303.5076
- Aloisi, A., Clementini, G., Tosi, M., et al. 2007, *ApJ*, 667, L151
- Asplund, M., Grevesse, N., Sauval, A. J., & Scott, P. 2009, *ARA&A*, 47, 481
- Aver, E., Olive, K. A., & Skillman, E. D. 2010, *J. Cosmol. Astropart. Phys.*, 5, 3
- Aver, E., Olive, K. A., & Skillman, E. D. 2011, *J. Cosmol. Astropart. Phys.*, 3, 43
- Aver, E., Olive, K. A., & Skillman, E. D. 2012, *J. Cosmol. Astropart. Phys.*, 4, 4
- Bastian, N., Covey, K. R., & Meyer, M. R. 2010, *ARA&A*, 48, 339
- Berg, D. A., Skillman, E. D., & Marble, A. R. 2011, *ApJ*, 738, 2
- Berg, D. A., Skillman, E. D., Marble, A. R., et al. 2012, *ApJ*, 754, 98
- Bohlin, R. C. 2010, *AJ*, 139, 1515
- Boselli, A., Boissier, S., Cortese, L., et al. 2009, *ApJ*, 706, 1527
- Bresolin, F., Gieren, W., Kudritzki, R.-P., et al. 2009, *ApJ*, 700, 309
- Brown, W. R., Kewley, L. J., & Geller, M. J. 2008, *AJ*, 135, 92
- Cannon, J. M., Skillman, E. D., Garnett, D. R., & Dufour, R. J. 2002, *ApJ*, 565, 931
- Cannon, J. M., Giovanelli, R., Haynes, M. P., et al. 2011, *ApJ*, 739, L22
- Cardelli, J. A., Clayton, G. C., & Mathis, J. S. 1989, *ApJ*, 345, 245
- Cole, A. A., Skillman, E. D., Tolstoy, E., et al. 2007, *ApJ*, 659, L17
- Crawford, D. L., & Barnes, J. V. 1970, *AJ*, 75, 978
- Croxall, K. V., van Zee, L., Lee, H., Skillman, E. D., Lee, J. C., Ct, S., Kennicutt, R. C., & Miller, B. W. 2009, *ApJ*, 705, 723
- Cyburt, R. H., Fields, B. D., & Olive, K. A. 2002, *Astroparticle Physics*, 17, 87
- Cyburt, R. H., Fields, B. D., & Olive, K. A. 2008, *J. Cosmol. Astropart. Phys.*, 11, 12
- Denicoló, G., Terlevich, R., & Terlevich, E. 2002, *MNRAS*, 330, 69
- Dohm-Palmer, R. C., Skillman, E. D., Gallagher, J., et al. 1998, *AJ*, 116, 1227
- Ekta, Chengalur, J. N., & Pustilnik, S. A. 2006, *MNRAS*, 372, 853
- Ekta, Chengalur, J. N., & Pustilnik, S. A. 2008, *MNRAS*, 391, 881
- Ekta, B., Pustilnik, S. A., & Chengalur, J. N. 2009, *MNRAS*, 397, 963
- Ekta, B., & Chengalur, J. N. 2010a, *MNRAS*, 403, 295
- Ekta, B., & Chengalur, J. N. 2010b, *MNRAS*, 406, 1238
- Fields, B. D., & Olive, K. A. 1998, *ApJ*, 506, 177
- Filippenko, A. V. 1982, *PASP*, 94, 715
- Fumagalli, M., da Silva, R. L., & Krumholz, M. R. 2011, *ApJ*, 741, L26
- Garnett, D. R. 1989, *ApJ*, 345, 282
- Garnett, D. R. 1990, *ApJ*, 363, 142
- Garnett, D. R. 1992, *AJ*, 103, 1330
- Giovanelli, R., Haynes, M.P., Kent, B.R., et al. 2005, *AJ*, 130, 2598
- Giovanelli, R., Haynes, M.P., Kent, B.R. & Adams, E.A.K. 2010, *ApJ*, 708, L22
- Giovanelli, R., Haynes, M.P., Adams, E.A.K., Cannon, J.M., Rhode, K.L., Salzer, J.J., Skillman, E.D., Bernstein-Cooper, E.Z., & McQuinn, K. 2013, *AJ*, submitted
- Guseva, N. G., Izotov, Y. I., Stasińska, G., et al. 2011, *A&A*, 529, A149
- Haynes, M. P., Giovanelli, R., Martin, A.M., et al. 2011, *AJ*, 142, 170
- Henry, R. B. C., Nava, A., & Prochaska, J. X. 2006, *ApJ*, 647, 984
- Hoversten, E. A., & Glazebrook, K. 2008, *ApJ*, 675, 163
- Hu, E. M., Cowie, L. L., Kakazu, Y., & Barger, A. J. 2009, *ApJ*, 698, 2014
- Hummer, D. G., & Storey, P. J. 1987, *MNRAS*, 224, 801
- Izotov, I. I., Guseva, N. G., Lipovetskii, V. A., Kniazev, A. I., & Stepanian, J. A. 1990, *Nature*, 343, 238
- Izotov, Y. I., Lipovetsky, V. A., Chaffee, F. H., et al. 1997, *ApJ*, 476, 698
- Izotov, Y. I., Chaffee, F. H., Foltz, C. B., et al. 1999, *ApJ*, 527, 757
- Izotov, Y. I., & Thuan, T. X. 1999, *ApJ*, 511, 639
- Izotov, Y. I., Thuan, T. X., & Guseva, N. G. 2005, *ApJ*, 632, 210
- Izotov, Y. I., Stasińska, G., Meynet, G., Guseva, N. G., & Thuan, T. X. 2006, *A&A*, 448, 955
- Izotov, Y. I., Thuan, T. X., & Stasińska, G. 2007, *ApJ*, 662, 15
- Izotov, Y. I., & Thuan, T. X. 2007, *ApJ*, 665, 1115
- Izotov, Y. I., & Thuan, T. X. 2010, *ApJ*, 710, L67
- Izotov, Y. I., Thuan, T. X., & Guseva, N. G. 2012, *A&A*, 546, A122
- Kakazu, Y., Cowie, L. L., & Hu, E. M. 2007, *ApJ*, 668, 853
- Kennicutt, R. C., Jr., Lee, J. C., Funes, S. J., José G., Sakai, S., & Akiyama, S. 2008, *ApJS*, 178, 247
- Kniazev, A. Y., Pustilnik, S. A., Masegosa, J., et al. 2000, *A&A*, 357, 101
- Kniazev, A. Y., Grebel, E. K., Hao, L., Strauss, M. A., Brinkmann, J., & Fukugita, M. 2003, *ApJ*, 593, L73
- Kobulnicky, H. A., & Skillman, E. D. 1996, *ApJ*, 471, 211
- Kobulnicky, H. A., & Skillman, E. D. 1997, *ApJ*, 489, 636
- Komatsu, E., Smith, K. M., Dunkley, J., et al. 2011, *ApJS*, 192, 18
- Kunth, D., Östlin, G. 2000, *A&A Rev.*, 10, 1
- Lee, J. C., Gil de Paz, A., Tremonti, C., et al. 2009, *ApJ*, 706, 599
- Lee, H., Skillman, E. D., & Venn, K. A. 2005, *ApJ*, 620, 223
- Lee, H., Skillman, E. D., & Venn, K. A. 2006b, *ApJ*, 642, 813
- Lee, H., Skillman, E. D., Cannon, J. M., Jackson, D. C., Gehrz, R. D., Polomski, E. F., & Woodward, C. E. 2006a, *ApJ*, 647, 970
- Lelli, F., Verheijen, M., Fraternali, F., & Sancisi, R. 2012, *A&A*, 537, A72
- Lequeux, J., Peimbert, M., Rayo, J. F., Serrano, A., & Torres-Peimbert, S. 1979, *A&A*, 80, 155
- Makarova, L. N., & Karachentsev, I. D. 1998, *A&AS*, 133, 181
- Massey, P., Stobel, K., Barnes, J. V., & Anderson, E. 1988, *ApJ*, 328, 315
- Mateo, M. L. 1998, *ARA&A*, 36, 435
- Matteucci, F., & Tosi, M. 1985, *MNRAS*, 217, 391
- McConnachie, A. W. 2012, *AJ*, 144, 4
- Melbourne, J., Phillips, A., Salzer, J. J., Gronwall, C., & Sarajedini, V. L. 2004, *AJ*, 127, 686
- Meurer, G. R., Wong, O. I., Kim, J. H., et al. 2009, *ApJ*, 695, 765
- Nakamura, K., et al. (Particle Data Group) 2010, *J. Phys. G: Nucl. Part. Phys.*, 37, 075021
- Nava, A., Casebeer, D., Henry, R. B. C., & Jevremovic, D. 2006, *ApJ*, 645, 1076
- Oke, J. B. 1990, *AJ*, 99, 1621
- Olive, K. A., & Skillman, E. D. 2001, *New Astronomy*, 6, 119
- Olive, K. A., & Skillman, E. D. 2004, *ApJ*, 617, 29
- Osterbrock, D. E., & Ferland, G. J. 2006, *Astrophysics of gaseous nebulae and active galactic nuclei*, 2nd. ed.: University Science Books
- Pagel, B. E. J. 1985, *European Southern Observatory Conference and Workshop Proceedings*, 21, 155
- Pagel, B. E. J., Simonson, E. A., Terlevich, R. J., & Edmunds, M. G. 1992, *MNRAS*, 255, 325
- Papaderos, P., Guseva, N. G., Izotov, Y. I., & Fricke, K. J. 2008, *A&A*, 491, 113
- Patat, F., Moehler, S., O'Brien, K., et al. 2011, *A&A*, 527, A91
- Peimbert, M., & Costero, R. 1969, *Boletín de los Observatorios Tonantzintla y Tacubaya*, 5, 3
- Peimbert, M., & Spinrad, H. 1970, *A&A*, 7, 311
- Peimbert, M., & Torres-Peimbert, S. 1974, *ApJ*, 193, 327
- Peimbert, M., Luridiana, V., & Peimbert, A. 2007, *ApJ*, 666, 636
- Peña-Guerrero, M. A., Peimbert, A., & Peimbert, M. 2012, *ApJ*, 756, L14
- Pettini, M., Zych, B. J., Steidel, C. C., & Chaffee, F. H. 2008, *MNRAS*, 385, 2011
- Pilyugin, L. S. 1993, *A&A*, 277, 42
- Pogge, R. W., Atwood, B., Brewer, D. F., et al. 2010, *Proc. SPIE*, 7735, 9
- Porter, R. L., Bauman, R. P., Ferland, G. J., & MacAdam, K. B. 2005, *ApJ*, 622, L73
- Porter, R. L., Ferland, G. J., & MacAdam, K. B. 2007, *ApJ*, 657, 327

- Porter, R. L., Ferland, G. J., Storey, P. J., & Detisch, M. J. 2012, *MNRAS*, 425, L28
- Porter, R. L., Ferland, G. J., Storey, P. J., & Detisch, M. J. 2013, *MNRAS*, in press, arXiv:1303.5115
- Pustil'nik, S. A., Lipovetsky, V. A., Izotov, Y. I., et al. 1997, *Astronomy Letters*, 23, 308
- Pustilnik, S. A., Kniazev, A. Y., & Pramskij, A. G. 2005, *A&A*, 443, 91
- Pustilnik, S. A., & Martin, J.-M. 2007, *A&A*, 464, 859
- Pustilnik, S. A., & Tepliakova, A. L. 2011, *MNRAS*, 415, 1188
- Pustilnik, S. A., Martin, J.-M., Tepliakova, A. L., & Kniazev, A. Y. 2011, *MNRAS*, 417, 1335
- Rhode, K.L., Salzer, J.J., Haurberg, N.C., Van Sistine, A., Young, M.D., Haynes, M.P., Giovanelli, R., Cannon, J.M., Skillman, E.D., McQuinn, K., & Adams, E.A.K. 2013, *AJ*, in press.
- Saviane, I., Rizzi, L., Held, E. V., Bresolin, F., & Momany, Y. 2002, *A&A*, 390, 59
- Schlafly, E. F., & Finkbeiner, D. P. 2011, *ApJ*, 737, 103
- Searle, L., & Sargent, W. L. W. 1972, *ApJ*, 173, 25
- Skillman, E. D., Kennicutt, R. C., & Hodge, P. W. 1989a, *ApJ*, 347, 875
- Skillman, E. D., & Kennicutt, R. C., Jr. 1993, *ApJ*, 411, 655
- Skillman, E. D., Terlevich, R., & Melnick, J. 1989b, *MNRAS*, 240, 563
- Stasińska, G. 1990, *A&AS*, 83, 501
- Stevenson, C. C., McCall, M. L., & Welch, D. L. 1993, *ApJ*, 408, 460
- Thuan, T. X., Izotov, Y. I., & Lipovetsky, V. A. 1995, *ApJ*, 445, 108
- Tolstoy, E., Gallagher, J. S., Cole, A. A., et al. 1998, *AJ*, 116, 1244
- Tolstoy, E., Hill, V., & Tosi, M. 2009, *ARA&A*, 47, 371
- Tremonti, C. A., Heckman, T. M., Kauffmann, G., Brinchmann, J., Charlot, S., White, S. D. M., Seibert, M., Peng, E. W., Schlegel, D. J., Uomoto, A., Fukugita, M., & Brinkmann, J. 2004, *ApJ*, 613, 898
- Tsujimoto, T., & Bekki, K. 2011, *A&A*, 530, A78
- Ugryumov, A. V., Engels, D., Pustilnik, S. A., et al. 2003, *A&A*, 397, 463
- van Dokkum, P., 2001, *PASP*, 113, 1420
- van Zee, L. 2000, *ApJ*, 543, L31
- van Zee, L., Haynes, M. P., & Salzer, J. J. 1997a, *AJ*, 114, 2479
- van Zee, L., Haynes, M. P., & Salzer, J. J. 1997b, *AJ*, 114, 2497
- van Zee, L., Westpfahl, D., Haynes, M. P., & Salzer, J. J. 1998, *AJ*, 115, 1000
- van Zee, L., & Haynes, M. P. 2006, *ApJ*, 636, 214
- van Zee, L., Skillman, E. D., & Haynes, M. P. 2006, *ApJ*, 637, 269
- Vilchez, J. M., & Pagel, B. E. J. 1988, *MNRAS*, 231, 257
- Walker, T. P., Steigman, G., Kang, H.-S., Schramm, D. M., & Olive, K. A. 1991, *ApJ*, 376, 51
- Weisz, D. R., Dalcanton, J. J., Williams, B. F., et al. 2011, *ApJ*, 739, 5
- Weisz, D. R., Johnson, B. D., Johnson, L. C., et al. 2012, *ApJ*, 744, 44
- Xia, L., Malhotra, S., Rhoads, J., et al. 2012, *AJ*, 144, 28

TABLE 1
EMISSION-LINE INTENSITIES AND EQUIVALENT
WIDTHS FOR LEO P

Ion	$I(\lambda)/I(H\beta)$	
	KPNO 4-m	LBT/MODS
[O II] $\lambda 3727$	0.467 \pm 0.038	0.465 \pm 0.017
H12 $\lambda 3750$...	0.038 \pm 0.007
H11 $\lambda 3771$	0.040 \pm 0.010	0.043 \pm 0.007
H10 $\lambda 3798$	0.045 \pm 0.010	0.055 \pm 0.008
He I $\lambda 3820$...	0.010 \pm 0.007
H9 $\lambda 3835$	0.062 \pm 0.009	0.072 \pm 0.007
[Ne III] $\lambda 3868$	0.118 \pm 0.011	0.106 \pm 0.008
He I+H8 $\lambda 3889$	0.195 \pm 0.015	0.197 \pm 0.009
[Ne III]+H7 $\lambda 3968$	0.181 \pm 0.014	0.186 \pm 0.009
He I $\lambda 4026$...	0.011 \pm 0.007
H δ $\lambda 4101$	0.253 \pm 0.015	0.268 \pm 0.009
H γ $\lambda 4340$	0.473 \pm 0.020	0.452 \pm 0.011
[O III] $\lambda 4363$	0.035 \pm 0.007	0.038 \pm 0.005
He I $\lambda 4471$	0.034 \pm 0.005	0.034 \pm 0.006
H β $\lambda 4861$	1.000 \pm 0.022	1.000 \pm 0.020
He I $\lambda 4921$...	0.009 \pm 0.006
[O III] $\lambda 4959$	0.468 \pm 0.010	0.482 \pm 0.010
[O III] $\lambda 5007$	1.399 \pm 0.031	1.453 \pm 0.030
He I $\lambda 5015$...	0.025 \pm 0.005
He I $\lambda 5876$	0.094 \pm 0.006	0.098 \pm 0.004
[S III] $\lambda 6312$...	0.007 \pm 0.003
[N II] $\lambda 6548$	0.008 \pm 0.004	0.009 \pm 0.003
H α $\lambda 6563$	2.699 \pm 0.197	2.750 \pm 0.095
[N II] $\lambda 6584$	0.021 \pm 0.005	0.025 \pm 0.003
He I $\lambda 6678$	0.026 \pm 0.006	0.028 \pm 0.003
[S II] $\lambda 6717$	0.047 \pm 0.007	0.036 \pm 0.003
[S II] $\lambda 6731$	0.027 \pm 0.006	0.027 \pm 0.003
He I $\lambda 7065$...	0.023 \pm 0.002
[Ar III] $\lambda 7136$...	0.026 \pm 0.002
He I $\lambda 7281$...	0.007 \pm 0.002
[O II] $\lambda 7320$...	0.006 \pm 0.002
[O II] $\lambda 7330$...	0.007 \pm 0.002
P13 $\lambda 8665$...	0.007 \pm 0.002
P12 $\lambda 8750$...	0.013 \pm 0.002
P11 $\lambda 8863$...	0.011 \pm 0.002
P10 $\lambda 9015$...	0.015 \pm 0.003
[S III] $\lambda 9069$...	0.043 \pm 0.004
P9 $\lambda 9229$...	0.020 \pm 0.003
[S III] $\lambda 9532$...	0.102 \pm 0.007
P8 $\lambda 9546$...	0.023 \pm 0.003
$C(H\beta)$	0.00 \pm 0.10	0.09 \pm 0.04
EW($H\beta$ (ABS)) (\AA)	2.0 \pm 2.0	1.0 \pm 2.0
$F(H\beta)$	46 \pm 0.7	34 \pm 0.7
EW($H\beta$) (\AA)	143	183
EW($H\alpha$) (\AA)	927	1222

NOTE. — Emission line fluxes (measured by directly integrating under the line profile and only using deblended Gaussian profile fits and multiple component fits when necessary) are relative to $H\beta = 1.00$ and are corrected for reddening. The $H\beta$ flux is given for reference, with units of $10^{-16} \text{ erg s}^{-1} \text{ cm}^{-2}$. Note that uncertainties listed in this table reflect the statistical uncertainties in the flux through the slit only, and do not account for slit losses.

TABLE 2
IONIC AND TOTAL ABUNDANCES FOR LEO P

Species	KPNO 4-m	LBT/MODS	Adopted
T(O ⁺⁺)	17150 $^{+2040}_{-1390}$	17350 $^{+1390}_{-1060}$...
T(O ⁺) (inferred)	14460 ± 1440	14530 ± 1030	...
T(S ⁺⁺) (inferred)	15930 ± 1190	16010 ± 1140	...
n _e (S ⁺)	0 $^{+235}_{-0}$ cm ⁻³	60 $^{+200}_{-60}$ cm ⁻³	...
n _e (O ⁺)	...	45 $^{+66}_{-45}$ cm ⁻³	...
(O ⁺ /H)	0.42 ± 0.13 × 10 ⁻⁵	0.41 ± 0.09 × 10 ⁻⁵	...
(O ⁺⁺ /H)	1.08 ± 0.22 × 10 ⁻⁵	1.09 ± 0.16 × 10 ⁻⁵	...
(O/H)	1.49 ± 0.26 × 10 ⁻⁵	1.50 ± 0.18 × 10 ⁻⁵	1.46 ± 0.14 × 10 ⁻⁵
log(O/H) + 12	7.17 ± 0.07	7.17 ± 0.05	7.17 ± 0.04
(N ⁺ /O ⁺)	4.0 ± 0.9 × 10 ⁻²	4.7 ± 0.6 × 10 ⁻²	4.4 ± 0.4 × 10 ⁻²
log(N/O)	-1.40 ± 0.09	-1.33 ± 0.05	-1.36 ± 0.04
(N ⁺ /H)	1.7 ± 1.1 × 10 ⁻⁷	2.0 ± 0.7 × 10 ⁻⁷	...
	ICF	3.58 ± 0.19	3.67 ± 0.13
(N/H)	5.9 ± 1.7 × 10 ⁻⁷	7.1 ± 1.2 × 10 ⁻⁷	6.7 ± 1.0 × 10 ⁻⁷
log(N/H) + 12	5.77 ± 0.11	5.85 ± 0.07	5.82 ± 0.06
(Ne ⁺⁺ /O ⁺⁺)	1.92 ± 0.25 × 10 ⁻¹	1.66 ± 0.14 × 10 ⁻¹	1.72 ± 0.12 × 10 ⁻¹
log(Ne/O)	-0.72 ± 0.05	-0.78 ± 0.04	-0.76 ± 0.03
(Ne ⁺⁺ /H)	2.07 ± 0.56 × 10 ⁻⁶	1.80 ± 0.35 × 10 ⁻⁶	...
	ICF	1.39 ± 0.19	1.37 ± 0.13
(Ne/H)	2.87 ± 0.62 × 10 ⁻⁶	2.48 ± 0.37 × 10 ⁻⁶	2.58 ± 0.32 × 10 ⁻⁶
log(Ne/H) + 12	6.46 ± 0.08	6.39 ± 0.06	6.42 ± 0.05
(S ⁺ /H)	0.75 ± 0.25 × 10 ⁻⁷	0.64 ± 0.12 × 10 ⁻⁷	...
(S ⁺⁺ /H)	...	2.84 ± 0.33 × 10 ⁻⁷	...
	ICF	1.39 ± 0.12	...
(S/H)	...	4.84 ± 0.55 × 10 ⁻⁷	4.84 ± 0.55 × 10 ⁻⁷
log(S/H) + 12	...	5.68 ± 0.47	5.68 ± 0.47
log(S/O)	...	-1.49 ± 0.07	-1.49 ± 0.07
(Ar ⁺⁺ /H)	...	9.1 ± 1.3 × 10 ⁻⁸	...
	ICF	1.65 ± 0.18	...
(Ar/H)	...	1.50 ± 0.27 × 10 ⁻⁷	1.50 ± 0.27 × 10 ⁻⁷
log(Ar/H) + 12	...	5.18 ± 0.07	5.18 ± 0.07
log(Ar/O)	...	-2.00 ± 0.09	-2.00 ± 0.09

TABLE 3
INPUTS AND χ^2 S FOR MCMC ANALYSIS OF HELIUM ABUNDANCE

Emission Line	Flux	EW	χ^2	+ $\lambda 5015 \chi^2$
H δ $\lambda 4101$	0.246 ± 0.006	26.5 ± 2.7	0.252	0.310
H γ $\lambda 4340$	0.431 ± 0.009	54.6 ± 5.5	2.751	2.686
H β $\lambda 4861$	1.000 ± 0.020	183.2 ± 18.3
H α $\lambda 6563$	2.949 ± 0.059	1222 ± 122	0.191	0.177
He I+H8 $\lambda 3889$	0.175 ± 0.007	16.3 ± 1.6	0.019	0.009
He I $\lambda 4026$	0.011 ± 0.007	1.0 ± 0.1	0.004	0.029
He I $\lambda 4471$	0.033 ± 0.006	4.5 ± 0.5	0.015	0.034
He I $\lambda 5015$	0.026 ± 0.006	5.0 ± 0.5	...	0.211
He I $\lambda 5876$	0.103 ± 0.004	30.2 ± 3.0	0.001	0.002
He I $\lambda 6678$	0.030 ± 0.003	14.3 ± 1.4	0.024	0.022
He I $\lambda 7065$	0.025 ± 0.003	12.8 ± 1.3	0.028	0.044
Total χ^2	3.29	3.50

NOTE. — Emission line fluxes are relative to H β = 1.00 and are *not* corrected for reddening (as reddening is derived in the MCMC analysis).

TABLE 4
MCMC ANALYSIS OF HELIUM ABUNDANCES AND
PHYSICAL CONDITIONS FOR LEO P

Parameter	Standard	+ $\lambda 5015$
Emission lines	9	10
Free Parameters	8	8
(He ⁺ /H ⁺)	0.0837 ^{+0.0084} _{-0.0062}	0.0837 ^{+0.0084} _{-0.0054}
T _e (10 ⁴ K)	1.71 ^{+0.19} _{-0.28}	1.72 ^{+0.18} _{-0.27}
n _e (cm ⁻³)	1 ⁺²⁰⁶ ₋₁	1 ⁺²⁰¹ ₋₁
C(H β)	0.10 ^{+0.03} _{-0.07}	0.10 ^{+0.03} _{-0.07}
a _H (EW Å)	0.94 ^{+1.44} _{-0.94}	1.02 ^{+1.43} _{-1.02}
a _{He} (EW Å)	0.50 ^{+0.42} _{-0.42}	0.45 ^{+0.39} _{-0.45}
τ_{He}	0.00 ^{+0.66} _{-0.00}	0.00 ^{+0.65} _{-0.00}
n _{HI} (10 ⁻⁴ cm ⁻³)	0 ⁺¹⁵⁶ ₋₀	0 ⁺¹⁵² ₋₀
χ^2	3.3	3.5
χ^2 /d.o.f.	3.3	1.75
Y	0.2509 ^{+0.0184} _{-0.0142}	0.2509 ^{+0.0184} _{-0.0123}